Thermosuperrepellency of a hot substrate caused by vapour percolation

J. Benedikt Schmidt
Technische Universitaet Darmstadt

Julian Hofmann
Technische Universitaet Darmstadt

Fabian Tenzer
Technische Universitaet Darmstadt

Jan Breitenbach
Technische Universitaet Darmstadt

Cameron Tropea
Technische Universität Darmstadt https://orcid.org/0000-0002-1506-9655

Ilia Roisman (roisman@sla.tu-darmstadt.de)
Technische Universitaet Darmstadt https://orcid.org/0000-0002-9878-3650

Article

Keywords:

Posted Date: August 14th, 2020

DOI: https://doi.org/10.21203/rs.3.rs-56255/v1

Version of Record: A version of this preprint was published at Communications Physics on August 13th, 2021. See the published version at https://doi.org/10.1038/s42005-021-00680-7.

Thermosuperrepellency of a hot substrate caused by vapour percolation

J. Benedikt Schmidt , Julian Hofmann , Fabian M. Tenzer , Jan Breitenbach , Cameron Tropea , and Ilia V. Roisman*

Technische Universitaet Darmstadt, Institute for Fluid Mechanics and Aerodynamics, Alarich-Weiss-Straße 10, Darmstadt, 64287, Germany
*roisman@sla.tu-darmstadt.de

Drop rebound after collision with a very hot substrate is usually attributed to the Leidenfrost effect,[1–5] characterized by intensive film boiling in a thin vapour gap between the liquid and substrate. Similarly, drop impact onto a cold superhydrophobic substrate[6–8] leads to a complete drop rebound, despite partial wetting of the substrate. We have studied the repellent properties of hot smooth hydrophilic substrates in the nucleate boiling, non-Leidenfrost regime and discovered that the thermally induced repellency is associated with vapour percolation on the substrate. The wetting structure in the presence of the percolating vapour rivulets is analogous to the Cassie-Baxter wetting mode,[9] which is a necessary condition for the repellency in the isothermal case. The theoretical predictions for the threshold temperature for vapour percolation agree well with the experimental data for drop rebound and correspond to the minimum heat flux when spray cooling.

In describing drop interaction with solid surfaces, researchers have reverted (unknowingly) to endowing drops and surfaces with the ability to empathize - drops spread with love on friendly hydrophilic substrates.* In contrast, drops impacting onto a fearful hydrophobic† or even superhydrophobic surfaces can often lead to rebound. What then does a drop "feel" when impacting onto an extremely hot substrate? Thermally induced drop rebound is one of the numerous observed impact outcomes,[10,11] which also include deposition, evaporation, breakup and atomization. These phenomena are substantially more complex and have to be described combining the hydrodynamic and thermodynamic aspects of the drop boiling on a hot substrate.

Drop spreading after impact onto a solid dry substrate is governed by the impact Reynolds number $Re \equiv \rho d_0 U_0/\mu$ and the Weber number $We \equiv \rho d_0 U_0^2/\sigma$, where ρ, μ and σ are the density, viscosity and surface tension of the liquid, d_0 is the initial drop diameter and U_0 is the impact velocity. Drop collision in the absence of thermal effects leads to the generation of a thin radially spreading lamella, bounded by a rim, formed by surface tension and the forces associated with the substrate wetting properties.[12,13]

Immediately after impact an expanding viscous boundary layer of thickness $\sim \sqrt{\nu t}$ is formed in the vicinity of the wall, where ν is the kinematic viscosity of the liquid. At some instant the thickness of the viscous boundary layer is equal to the lamella thickness. At subsequent times the flow in the lamella is quickly damped by the viscosity. The theoretically predicted residual lamella thickness and the characteristic time of spreading governed by viscosity are obtained in the form[14]

$$h_{\text{res}} \approx 0.79 d_0 Re^{-2/5}, \quad t_\nu \sim \frac{d_0 Re^{1/5}}{U_0}. \tag{1}$$

For lower Weber number the effect of surface tension becomes dominant and the rim can start to recede before the cessation of the flow in the lamella. In many cases, for example in the film boiling regime,[15] in the case of drop impact onto a superhydrophobic substrate,[16] or binary drop collisions,[17] the spreading time is scaled very well with the typical time of drop natural oscillations

$$t_\sigma \approx \sqrt{\frac{\rho d_0^3}{\sigma}} = \frac{d_0 We^{1/2}}{U_0}. \tag{2}$$

The viscous spreading regime corresponds to the case $t_\nu \ll t_\sigma$, namely when $We \gg Re^{2/5}$.

In the case of drop impact onto a hot substrate two thermal boundary layers, in the solid substrate and in the liquid flow, start to expand in the vicinity of the liquid/solid interface.[18] If the substrate initial temperature T_{wall} is well above the saturation point T_{sat}, the flow is accompanied by the heterogeneous nucleation of the vapour bubbles.[19,20] In this regime the wall temperature near the evaporating contact line of each bubble approaches T_{sat}. The heat flux $\dot{q}$ in the nucleate boiling regime is then estimated[21] from the well-known solution of the conduction problem in the wall

$$\dot{q} = \frac{e_w \Delta T_w}{\sqrt{\pi t}}. \tag{3}$$

The total evaporation time of the deposited drop can now be estimated using (3) from the balance of the total heat required for the complete drop evaporation and the heat transferred from the substrate[21]

$$t_{\varepsilon\text{drop}} = \pi \left(\frac{\rho L^* d_0}{12 k_w e_w \Delta T_w} \right)^2, \quad \Delta T_w = T_{\text{wall}} - T_{\text{sat}}, \tag{4}$$

in which k_w is a dimensionless empirical constant of the order of unity, associated with the surface wettability, e_w is the thermal effusivity of the substrate and $L^* = L + \Delta H_0$ is the sum of the latent heat of evaporation L and the enthalpy difference ΔH_0 between the initial drop and saturated liquid.

Typical phenomena of drop impact onto a substrate at various initial temperatures, captured using a high-speed video system, are shown in Fig. 1**a**-**c**. The contact residence time t_r of an impacting drop is determined either by the instant of drop rebound or by the duration of complete evaporation of a deposited drop and is shown in Fig. 1**d** as a function of the initial substrate overheat $T_{\text{wall}} - T_{\text{sat}}$. Three main outcomes of drop impact in the nucleate boiling regime include drop deposition and complete evaporation (one example is shown in Fig. 1**a**), complete rebound after a certain delay due to a short period of sticking to the substrate (illustrated by the example in Fig. 1**b**), and non-sticking rebound (Fig. 1**c**). As shown in the graph in Fig. 1**d**, the contact residence time t_r of the deposited drop in the nucleate boiling regime (here for $\Delta T_{\text{wall}} < 50\,^\circ\text{C}$) marked by

*The word hydrophilic is formed from the ancient Greek words ὕδωρ and φιλία for water and love.

†From the Greek ὑδρόφοβος, terrified by water.

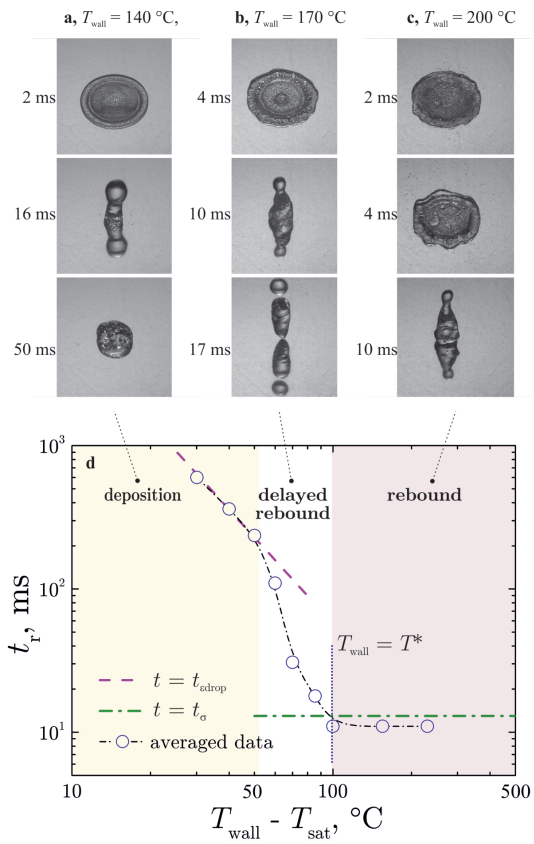

Figure 1. Typical stages and main outcomes of drop impact onto a hot solid substrate at various initial temperatures. The $d_0 = 2.35$ mm drop impacting onto an aluminium substrate with the impact velocity $U_0 = 2$ m/s. Figures **a**, **b**, and **c** are exemplary images of drop impact captured using a high-speed video system. **a**, drop impact at $T_{\text{wall}} = 140°\text{C}$ shows drop spreading, receding and deposition in the nucleate boiling regime. The contact residence time is determined by complete drop evaporation; **b**, $T_{\text{wall}} = 170°\text{C}$, intensive nucleate boiling leads to the drop rebound delayed by a short period of sticking (see the image at 10 ms); **c**, $T_{\text{wall}} = 200°\text{C}$, non-sticking drop rebound; **d**, Dependence of the average contact residence time t_r on the wall overheat temperature ΔT_w in comparison with the theoretical estimations for $t_{\varepsilon\text{drop}}$ and t_σ. Each experimental point is the average value of 10 experiments for the corresponding temperature class.

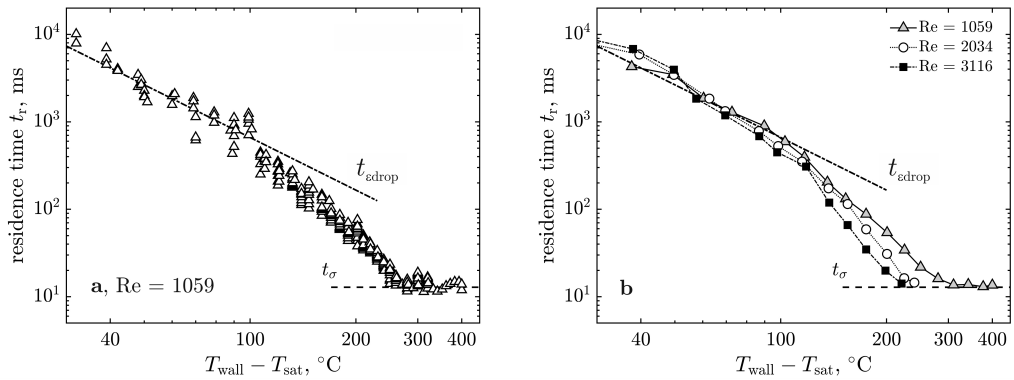

Figure 2. Parametric study of the residence time of an impacting water drop. Steel target. a, Experimental results on the residence time t_r. Each symbol corresponds to a single drop impact onto a steel target with various initial temperatures. The impact parameters are $d_0 = 2.3$ mm and $U_0 = 0.46$ m/s. **b**, Residence time t_r averaged over a target temperature class for different impact velocities.

the yellow color, agrees well with the theoretical predictions (4). In the range of highest wall temperatures ($\Delta T_w > 100\,°$C, pink region in Fig. 1) the residence time is very close to the drop capillary time t_σ defined in Eq. (2) due to the non-sticking drop rebound. However, in the intermediate range of the temperatures ($50\,°\text{C} < \Delta T_w < 100\,°\text{C}$) the residence time t_r deviates significantly from both $t_{\varepsilon\text{drop}}$ and t_σ. The delay of the drop rebound in this regime is caused by the bonding of the drop at residual wetted spots of the target, as in the 10 ms frame in Fig. 1**b**.

The residence time is significantly influenced by the thermal properties of the substrate, its initial temperature as well as by the impact parameters. In Fig. 2 the results of the measurements of t_r on the steel target are also shown in comparison with the theoretically predicted times $t_{\varepsilon\text{drop}}$ and t_σ. While in Fig. 2**a** the residence time for a certain set of impact parameters are shown, in Fig. 2**b** the value of t_r is shown averaged over a substrate temperature class.

Let us denote T^* as the lowest wall temperature at which the drop does not stick to the substrate. This point corresponds to the local minimum in the total heat, $Q = \int_0^{t_r} A(t)\dot{q}(t)\mathrm{d}t$ transferred from the substrate during drop impact, since the heat increases with the residence time and with the wall temperature. Here $A(t)$ is the wetted area of the substrate. We can thus expect that the heat flux during spray cooling at the threshold point T^* will also be minimal.

In Fig. 3**a** the evolution of the heat flux $\dot{q}$ and the interface temperature T_i of a thick stainless steel target continuously cooled by spray impact are shown. The target is initially heated uniformly up to $T_\text{w} \approx 450\,°$C. The high-speed observations of spray impact, shown in the inserts in Fig. 3**a**, demonstrate that the threshold temperature T^* associated with the minimum of the heat flux curve indeed determines the deposition/rebound limit for the impacting drops.

The value of the threshold temperature T^* depends neither on the drop diameter in the spray nor on the impact velocity, but on the target material, as is demonstrated in Figs. 3**b** and **c**. Moreover, no dependence of the temperature T^* on the mass flux of the impacting spray or other impact properties has been identified.

In Fig. 4 details are shown of the development of the vapour phase in the advanced nucleate boiling regime, which allow us to better understand the mechanisms of a single drop rebound. Fig. 4**a** clearly shows the vapour bubbles on the aluminium substrate at $T_\text{wall} = 170°$C and in **b** the formation of elongated vapour rivulets at higher temperatures, $T_\text{wall} = 200°$C, at which drops rebound without delay. The impact parameters in Figs. 4**a** and **b** are the same as in Fig. 1. Fig. 4**c** is the map of the heat flux distribution at the surface of a transparent sapphire target at $T_\text{wall} = 378°$C during drop spreading.[22] The wall temperature is well above the threshold temperature T^*. The red spots, corresponding to high local heat flux, indicate wetting of the substrate. The green or blue regions of low heat flux indicate the percolated vapour rivulets, similar to those observed in Fig. 4**b**.

The randomly distributed disks on a plane in Fig. 4**c** is an exemplary illustration of the irregular nucleation of bubbles. The spatial distribution of disks is characterized by the cumulative relative area λ of the disks, scaled by the total area of the domain. The percolation threshold in this two-dimensional problem[23] is $\lambda_c = 1.128$. At this point an infinite cluster of the intersecting disks first appears, as shown in Fig. 4**d**. The formation of the wrapping cluster of the disks at the percolation threshold can explain the percolation of the vapour bubbles and formation of the vapour rivulets. The computed value $\lambda_c = 1.128$ is only a very rough approximation for the percolation threshold for the vapour bubbles, since the model does not consider bubble coalescence or shear driven motion of the bubbles in the liquid flow.

The relative wetted surface area (not belonging to the surface covered by the bubbles), ε, can be estimated assuming a

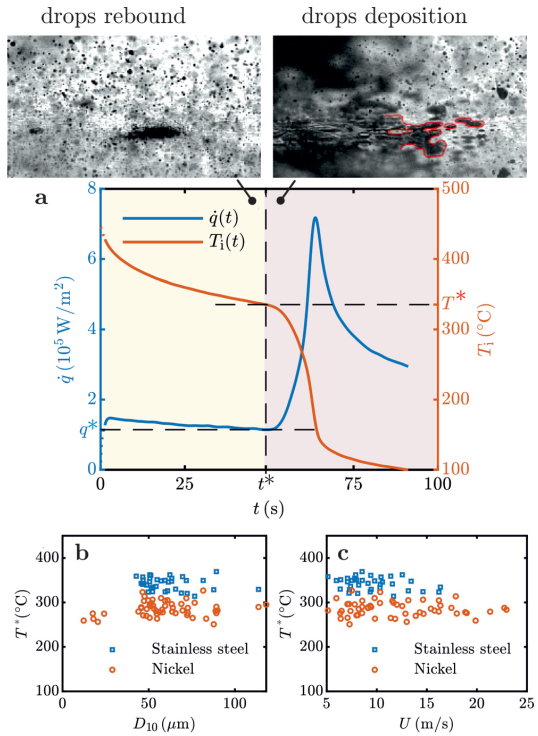

Figure 3. The threshold temperature T^* for spray impact. **a**, Exemplary results for the evolution of the heat flux $\dot{q}$ and surface temperature T_i as a function of time t for spray cooling with distilled water. The threshold temperature T^* at the instant t^* corresponds to the minimum heat flux. Inserts show liquid patterns on the surface shortly above and below the threshold temperature T^*. **b** and **c**, The dependence of the threshold temperature T^* on the average drop diameter D_{10} in the spray and on the average impact velocity U, respectively.

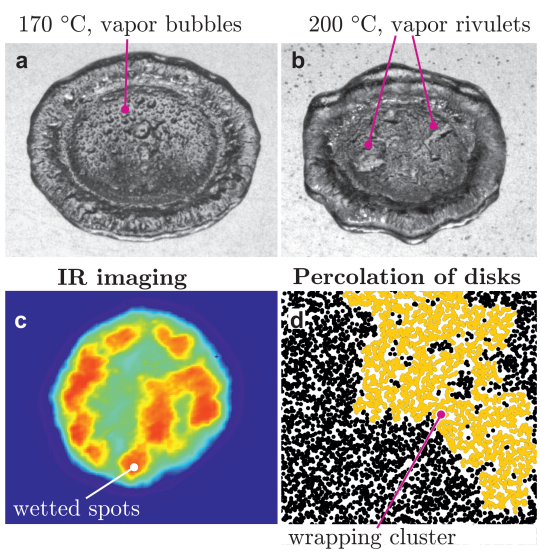

Figure 4. Boiling of the liquid lamella on a hot substrate. **a**, Spreading of the drop in the delayed rebound regime, $T_{\text{wall}} = 170°\text{C}$, captured by the high-speed video system. Bubbles are the result of the heterogeneous nucleation at the substrate. **b**, Appearance of the percolating vapour rivulets at $T_{\text{wall}} = T^* = 200°\text{C}$. This impact leads to a non-sticking rebound. **c**, Heat flux map, computed using the images captured using the high-speed infrared camera during drop impact onto a sapphire target at $T_{\text{wall}} = 378°\text{C}$, corresponding to the non-sticking rebound accompanied by the intensive generation of fine secondary drops. The red regions of peak heat flux correspond to the substrate wetting. **d**, Visualization of a continuum percolation with randomly distributed disks at $\lambda = 1.2$, slightly above the percolation threshold λ_c. The wrapping cluster is marked by the orange color.

Poisson distribution of the bubble positions.[24] At the percolation threshold it yields

$$\varepsilon_c = \exp(-\lambda_c) \approx 0.32. \tag{5}$$

The flow in the drop for values of relative volume of the liquid phase $\varepsilon > \varepsilon_c$ is completely different since the liquid contacts the substrate only at isolated wetted spots, which cannot prevent drop rebound, as in Fig. 1**c**. Let us roughly estimate the wall temperature corresponding to the emergence of the percolating vapour channels during the spreading time t_σ. Consider the liquid lamella of the thickness h_{res} defined in Eq. (1). It can be estimated from the one-dimensional energy balance accounting for the creation of the vapour phase, expressed as

$$\rho h_{\text{res}} L \varepsilon'(t) = -\dot{q}\varepsilon(t), \tag{6}$$

where ε is the relative volume of the liquid phase in the lamella. The solution of this differential equation is

$$\varepsilon(t) = \exp\left[-\frac{1.43 e_w \Delta T_w t^{1/2}}{\rho d_0 L Re^{2/5}}\right]. \tag{7}$$

With the help of (2) (3) and (5) the condition $\varepsilon = \varepsilon_c$ at the instant $t = t_\sigma$ yields the following expression for the threshold overheat ΔT_σ in the surface tension driven spreading regime

$$\Delta T_\sigma = 0.8 \frac{d_0^{1/4} L^* \rho^{3/4} \sigma^{1/4}}{e_w Re^{2/5}}. \tag{8}$$

For very high Weber numbers the duration of drop spreading is scaled by the viscous time scale t_ν, defined in (1). The percolation condition $\varepsilon = \varepsilon_c$ at the instant $t = t_\nu$ yields another expression for the threshold wall overheat ΔT_ν in the viscous spreading regime

$$\Delta T_\nu = \frac{\rho \sqrt{\nu} L^*}{e_w}. \tag{9}$$

It should be noted that the Leidenfrost phenomenon can be initiated as soon as the value of the relative wetted area approaches zero, $\varepsilon \ll 1$. Therefore, the Leidenfrost point can also be described using the scales defined in (8) and (9), depending on the drop impact parameters.

The expression for ΔT_ν does not depend on the drop diameter or impact velocity. This is not surprising, since the time t_ν and the lamella thickness h_{res} correspond to the one-dimensional growth of the viscous boundary layer in the lamella. This means that expression (9) can be used for the prediction of the Leidenfrost point even for a stationary (sessile) drop.

In Fig. 5 the theoretically predicted scales for the threshold temperature ΔT_σ and ΔT_ν are compared with the experimental data. The data for low speed impacts with $We < 2.5 Re^{2/5}$, governed by surface tension, are shown in Fig. 5**a** as a function of ΔT_σ. The agreement is good, considering that the target materials and the impact velocities have been widely varied in the experiments.

The effect of surface tension on the drop kinematics is negligibly small if $We > 2.5 Re^{2/5}$ and also for stationary drops. The threshold temperature in these cases, ΔT^*, has to correlate with ΔT_ν, which accounts for the expansion of the viscous boundary layer in the drop. The graphs in Figs. 5**b** and **c** confirm this assumption. All three graphs in Fig. 5 demonstrate a linear dependence of the data on the theoretical predictions. Moreover, the slope of the straight fitting line is in all the cases comparable with unity. This result demonstrates that the main physical players responsible for the thermosuperrepellency are correctly identified in our model.

Several hypotheses have been put forward in the literature to explain the mechanism of film boiling. Some theoretical models have been developed based on the hydrodynamic stability analysis of the vapour/liquid interface[25,26] or thermocapillary stability.[27] Other authors assume that the Leidenfrost temperature is determined by the foam limit[28,29] or by the limiting minimum vapour thickness[30] comparable with the surface roughness. In this study we have demonstrated that the transition to the film boiling regime is initiated at the threshold point for vapour percolation. Further drop evaporation is governed by the presence of the vapour rivulets and is characterized by the disappearance of the isolated wetted spots. The film boiling regime corresponds to a complete vanishing of the wetted spots.

Experimental methods

Two main experimental setups are used to observe single drop impact and to characterize spray cooling of hot substrates. They are shown schematically in Fig. 6.

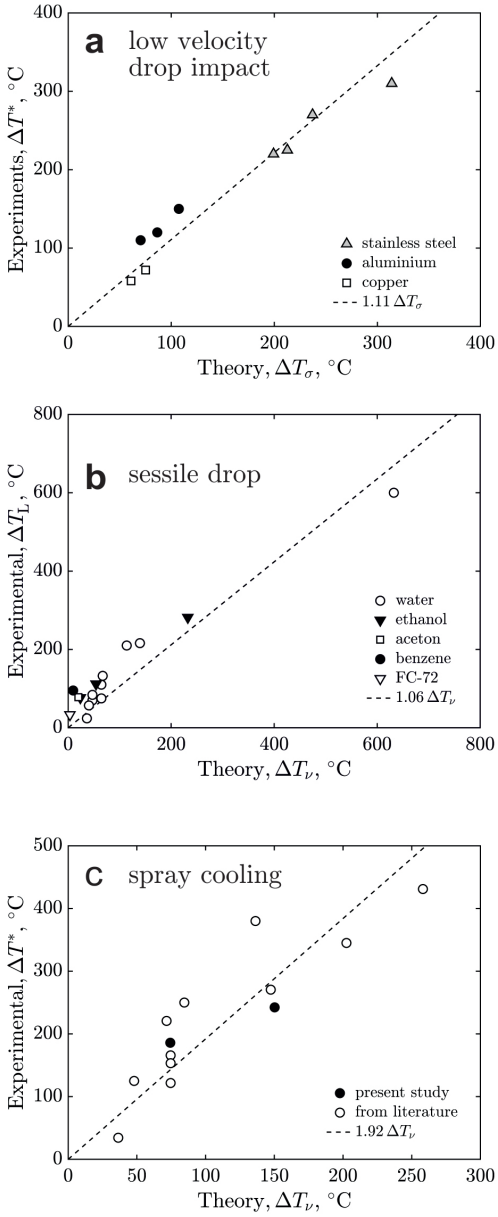

Figure 5. Comparison of the threshold overheat temperatures $\Delta T^* \equiv T^* - T_{\mathrm{sat}}$ with the theoretically predicted scales ΔT_σ and ΔT_ν. a, Data for low velocity single drop impact with $We < 2.5Re^{2/5}$, governed by surface tension, as a function of ΔT_σ defined in (8); **b**, The existing data from the literature for the Leidenfrost point ΔT_{L} for sessile drops of different liquids and substrates as a function of ΔT_ν; **c**, Data for water spray cooling of targets of different materials and for the high-speed single drop impacts with $We > 2.5Re^{2/5}$, governed by the viscosity, as a function of ΔT_ν. The data for different liquids from this study and from the literature are listed in the Supplementary Material.[22]

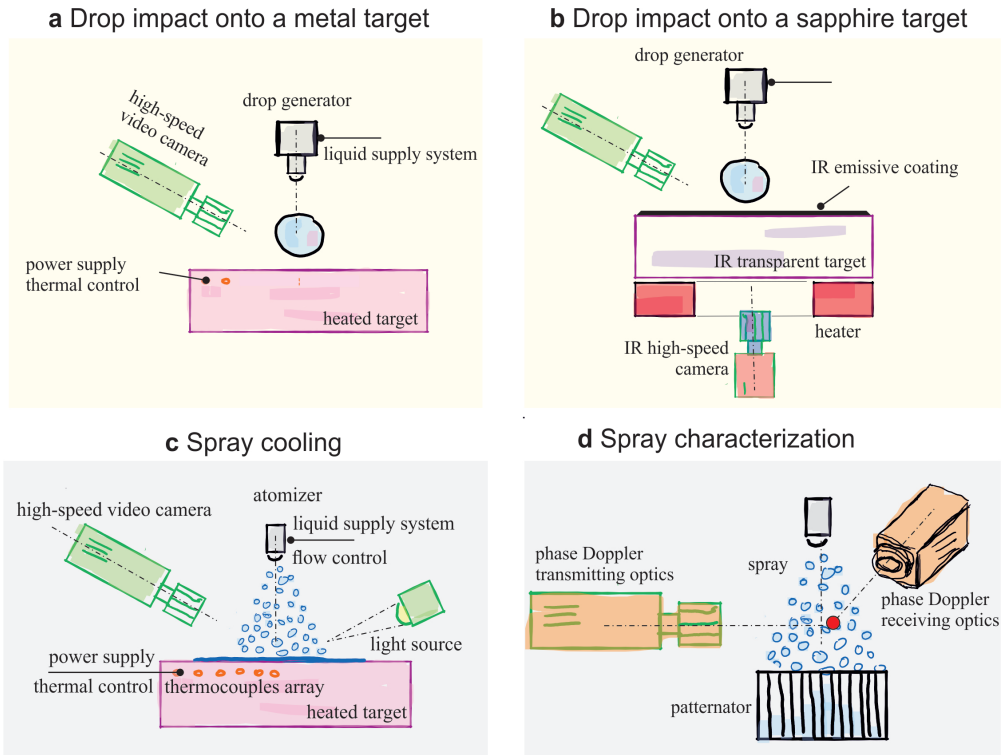

Figure 6. Sketches of the experimental setups for the single drop and spray cooling experiments. **a**, The setup consists of an adjustable drop generation unit, a heated impact target and a high-speed observation system. The heater and impact target are replaced for IR measurements during the drop impact. **b**, The setup for infrared (IR) measurements. The heater provides bottom view optical access for a high-speed infrared camera. **c**, Setup for characterization of spray cooling . **d**, Setup for detailed spray characterization.

Observations of single drop impact onto a hot substrate Two configurations of the experimental setup for a single drop impact are used in this study, one is to study the outcome of drop impact onto metal targets (Fig. 6**a**) and the other is for the high-speed thermographic visualization of the substrate interface exposed to the collision of a drop (Fig. 6**b**).

Single drops of double-distilled water with a diameter of $d_0 = 2.3\,\mathrm{mm}$ are generated by a drop-on-demand generator (as shown in Fig. 6**a**). The drop generator is cooled to maintain the liquid temperature constant at $20\,^{\circ}\mathrm{C}$. By changing the height, the impact velocity can be changed in the range of $U_0 = 0.4$ to $2\,\mathrm{m\,s^{-1}}$. Various target materials are used to identify the influence of the material properties on the drop impact outcome: aluminium (EN AW 7075), copper (CW004A) or stainless steel (1.4841). The replaceable impact substrates are heated by a heating device. The surface temperature is measured with a type J thermocouple 1 mm below the surface. The drop impact is observed using a high-speed video system, consisting of a CMOS camera and background illumination.

The setup for the visualization of the micro-scale thermodynamic effects at the drop-substrate interface and for the measurements of the temperature distribution is shown in Fig 6**b**. The high-speed thermographic measurements are performed using a mid-wave infrared camera. The bottom view of the wetted interface is achieved by using an infrared (IR) transparent sapphire target. The impact surface of the target is coated with a thin highly infrared emissive CrN PVD layer.

The heat flux at the substrate interface is then obtained by a numerical solution of the heat conduction problem in the sapphire substrate, satisfying the boundary conditions for the evolution of the temperature distribution obtained from the thermographic measurements.

Spray Cooling setup The experimental setup, as shown in Fig. 6**c**, consists of a heated target, a spraying system, a high-speed visual observation system and a spray characterization system. The temperature distribution in the target, heated using cartridge heaters, is measured by a set of the thermocouples placed in two rows at different depths from the surface. These temperatures are used for computation of the local heat flux and instantaneous surface temperature by solution of the inverse heat conduction problem.[31] To determine the effect of the wall thermal properties on the Leidenfrost point, two targets of different materials, stainless steel and nickel, have been used.

To identify the effect of the main spray parameters on the cooling rate, the average drop diameter, average velocity and the

mass flux density of the spray have been varied in the experiments. They are accurately characterized using a phase Doppler system and a custom built patternator, as schematically shown in Fig. 6**d**. The phase Doppler measurements were performed without the target, but at positions corresponding to specific locations immediately above the target; hence the spray parameters were local values. A high-speed camera equipped with a long distance microscope allows observation of the hydrodynamic phenomena at the target surface during spray impact.

The brief description of the materials can be found in the Supplementary Material.[22]

References

1. Leidenfrost, J. G. *De aquae communis nonnullis qualitatibus tractatus* (Ovenius, Duisburg ad Rhenum, 1756).
2. Gottfried, B., Lee, C. & Bell, K. The Leidenfrost phenomenon: film boiling of liquid droplets on a flat plate. *Int. J. heat mass transfer* **9**, 1167–1188 (1966).
3. Chandra, S. & Avedisian, C. On the collision of a droplet with a solid surface. *Proc. R. Soc. Lond. Ser. A-Math. Phys. Eng. Sci.* **432**, 13–41 (1991).
4. Biance, A.-L., Clanet, C. & Quéré, D. Leidenfrost drops. *Phys. fluids* **15**, 1632–1637 (2003).
5. Quéré, D. Leidenfrost dynamics. *Annu. Rev. Fluid Mech.* **45**, 197–215 (2013).
6. Renardy, Y. *et al.* Pyramidal and toroidal water drops after impact on a solid surface. *J. Fluid Mech.* **484**, 69–83, DOI: 10.1017/S0022112003004142 (2003).
7. Bird, J. C., Dhiman, R., Kwon, H.-M. & Varanasi, K. K. Reducing the contact time of a bouncing drop. *Nature* **503**, 385–388 (2013).
8. Liu, Y. *et al.* Pancake bouncing on superhydrophobic surfaces. *Nat. physics* **10**, 515–519 (2014).
9. Quéré, D. Non-sticking drops. *Reports on Prog. Phys.* **68**, 2495 (2005).
10. Bertola, V. An impact regime map for water drops impacting on heated surfaces. *Int. J. Heat Mass Transf.* **85**, 430–437, DOI: 10.1016/j.ijheatmasstransfer.2015.01.084 (2015).
11. Liang, G. & Mudawar, I. Review of spray cooling – Part 2: H- igh temperature boiling regimes and quenching applications. *Int. J. Heat Mass Transf.* **115**, 1206–1222, DOI: 10.1016/j.ijheatmasstransfer.2017.06.022 (2017).
12. Roisman, I. V., Rioboo, R. & Tropea, C. Normal impact of a liquid drop on a dry surface: model for spreading and receding. *Proc. R. Soc. Lond. Ser. A-Math. Phys. Eng. Sci.* **458**, 1411–1430 (2002).
13. Yarin, A. L., Roisman, I. V. & Tropea, C. *Collision phenomena in liquids and solids* (Cambridge University Press, 2017).
14. Roisman, I. V. Inertia dominated drop collisions. II. An analytical solution of the Navier–Stokes equations for a spreading viscous film. *Phys. Fluids* **21**, 052104 (2009).
15. Senoner, J.-M., Castanet, G., Caballina, O. & Villedieu, P. Modeling of water drop impactions in the Leidenfrost regime. *Atom. Sprays* **26** (2016).
16. Richard, D., Clanet, C. & Quéré, D. Contact time of a bouncing drop. *Nature* **417**, 811–811 (2002).
17. Willis, K. & Orme, M. Binary droplet collisions in a vacuum environment: an experimental investigation of the role of viscosity. *Exp. Fluids* **34**, 28–41 (2003).
18. Roisman, I. V. Fast forced liquid film spreading on a substrate: flow, heat transfer and phase transition. *J. Fluid Mech.* **656**, 189 (2010).
19. Itaru, M. & Kunihide, M. Heat transfer characteristics of evaporation of a liquid droplet on heated surfaces. *Int. journal heat mass transfer* **21**, 605–613 (1978).
20. Abu-Zaid, M. An experimental study of the evaporation characteristics of emulsified liquid droplets. *Heat mass transfer* **40**, 737–741 (2004).
21. Breitenbach, J., Roisman, I. V. & Tropea, C. Drop collision with a hot, dry solid substrate: Heat transfer during nucleate boiling. *Phys. Rev. Fluids* **2**, DOI: 10.1103/PhysRevFluids.2.074301 (2017).
22. See Supplementary Material [in the separate file] for detailed description of the experimental method and for the list of the experimental data from the literature.
23. Mertens, S. & Moore, C. Continuum percolation thresholds in two dimensions. *Phys. Rev. E* **86**, 061109 (2012).
24. Feller, W. *An introduction to probability theory and its applications, vol 2* (John Wiley & Sons, 2008).

25. Zuber, N. On the stability of boiling heat transfer. *Trans. Am. Soc. Mech. Engrs.* **80** (1958).

26. Kakac, S. & Bon, B. A review of two-phase flow dynamic instabilities in tube boiling systems. *Int. J. Heat Mass Transf.* **51**, 399–433, DOI: 10.1016/j.ijheatmasstransfer.2007.09.026 (2008).

27. Aursand, E., Davis, S. H. & Ytrehus, T. Thermocapillary instability as a mechanism for film boiling collapse. *J. Fluid Mech.* **852**, 283–312, DOI: 10.1017/jfm.2018.545 (2018).

28. Spiegler, P., Hopenfeld, J., Silberberg, M., Bumpus, C. F. & Norman, A. Onset of stable film boiling and the foam limit. *Int. J. Heat Mass Transf.* **6**, 987–989, DOI: 10.1016/0017-9310(63)90053-X (1963).

29. Wang, Z., Qu, W., Xiong, J., Zhong, M. & Yang, Y. Investigation on effect of surface properties on droplet impact cooling of cladding surfaces. *Nucl. Eng. Technol.* DOI: 10.1016/j.net.2019.08.022 (2019).

30. Cai, C., Mudawar, I., Liu, H. & Si, C. Theoretical Leidenfrost point (LFP) model for sessile droplet. *Int. J. Heat Mass Transf.* **146**, 118802, DOI: 10.1016/j.ijheatmasstransfer.2019.118802 (2020).

31. Woodfield, P. L., Monde, M. & Mitsutake, Y. Improved analytical solution for inverse heat conduction problems on thermally thick and semi-infinite solids. *Int. J. Heat Mass Transf.* **49**, 2864–2876, DOI: 10.1016/j.ijheatmasstransfer.2006.01.050 (2006).

Acknowledgements

The authors gratefully acknowledge the Deutsche Forschungsgemeinschaft for its financial support in the framework of the project SFB-TRR 75, project number 84292822 and the Industrieverband Massivumformung e.V..

Author contributions

C.T. and I.V.R. conceived the project. J.B.S. and J.B performed the single drop experiments. J.H. and F.M.T. performed the spray cooling experiments. C.T. was responsible for the scientific coordination of the project. I.V.R developed theoretical description of the problem. All authors performed the data analysis and participated in writing the manuscript.

Correspondence

Correspondence and requests for materials should be addressed to I.V.R.

Competing interests

The authors declare no competing interests.

Figures

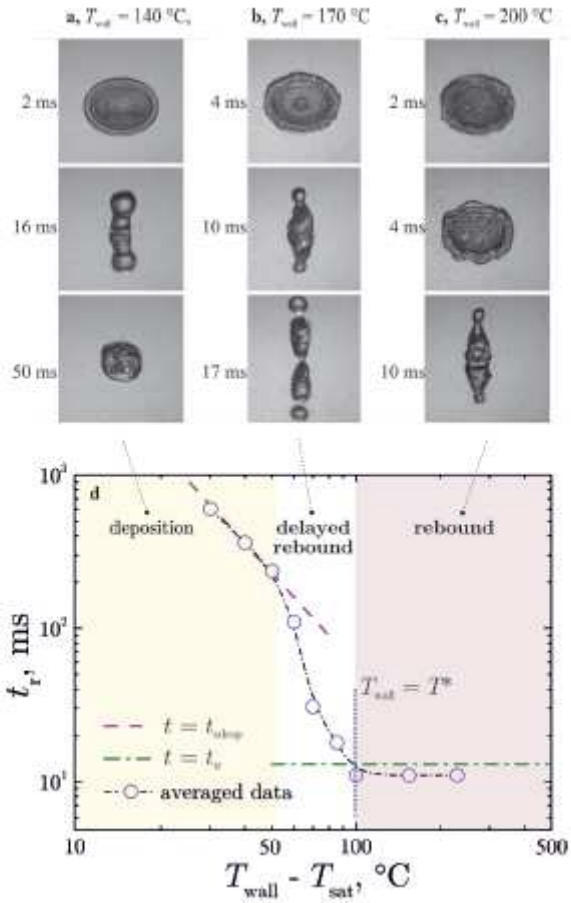

Figure 1

Typical stages and main outcomes of drop impact onto a hot solid substrate at various initial temperatures. The d0 = 2:35 mm drop impacting onto an aluminium substrate with the impact velocity U0 = 2 m/s. Figures a, b, and c are exemplary images of drop impact captured using a high-speed video system. a, drop impact at Twall = 140°C shows drop spreading, receding and deposition in the nucleate boiling regime. The contact residence time is determined by complete drop evaporation; b, Twall = 170°C, intensive nucleate boiling leads to the drop rebound delayed by a short period of sticking (see the image at 10 ms); c, Twall = 200°C, non-sticking drop rebound; d, Dependence of the average contact residence time tr on the wall overheat temperature DTw in comparison with the theoretical estimations for tedrop and ts . Each experimental point is the average value of 10 experiments for the corresponding temperature class.

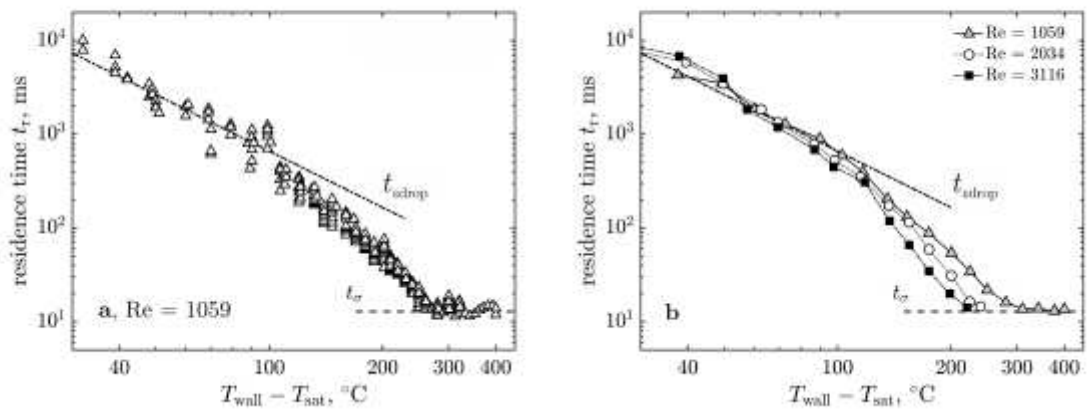

Figure 2

Parametric study of the residence time of an impacting water drop. Steel target. a, Experimental results on the residence time tr. Each symbol corresponds to a single drop impact onto a steel target with various initial temperatures. The impact parameters are d0 = 2:3 mm and U0 = 0:46 m/s. b, Residence time tr averaged over a target temperature class for different impact velocities.

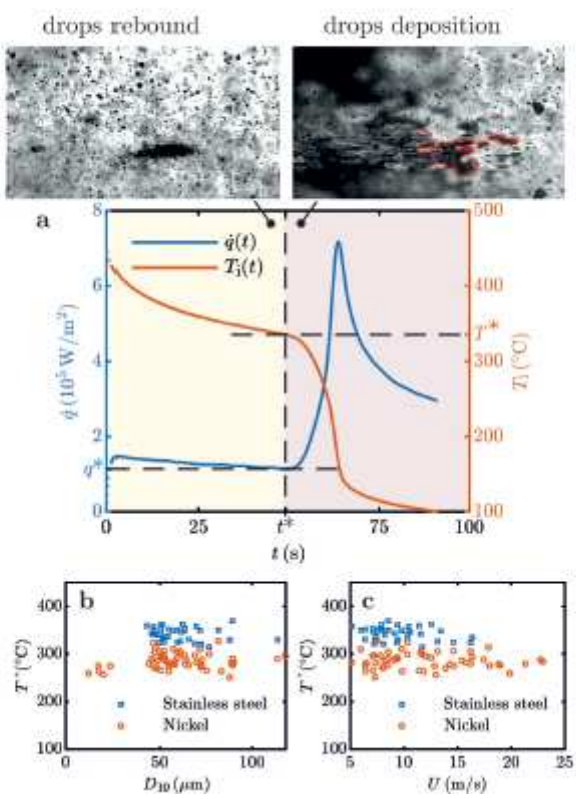

Figure 3

The threshold temperature T□ for spray impact. a, Exemplary results for the evolution of the heat flux ˙ q and surface temperature Ti as a function of time t for spray cooling with distilled water. The threshold

temperature T□ at the instant t□ corresponds to the minimum heat flux. Inserts show liquid patterns on the surface shortly above and below the threshold temperature T□. b and c, The dependence of the threshold temperature T□ on the average drop diameter D10 in the spray and on the average impact velocity U, respectively.

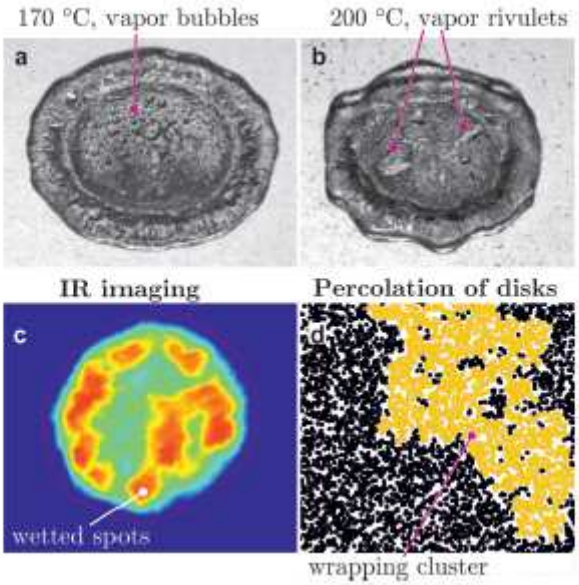

Figure 4

Boiling of the liquid lamella on a hot substrate. a, Spreading of the drop in the delayed rebound regime, Twall = 170□C, captured by the high-speed video system. Bubbles are the result of the heterogeneous nucleation at the substrate. b, Appearance of the percolating vapour rivulets at Twall = T□ = 200□C. This impact leads to a non-sticking rebound. c, Heat flux map, computed using the images captured using the high-speed infrared camera during drop impact onto a sapphire target at Twall = 378□C, corresponding to the non-sticking rebound accompanied by the intensive generation of fine secondary drops. The red regions of peak heat flux correspond to the substrate wetting. d, Visualization of a continuum percolation with randomly distributed disks at l = 1:2, slightly above the percolation threshold lc. The wrapping cluster is marked by the orange color.

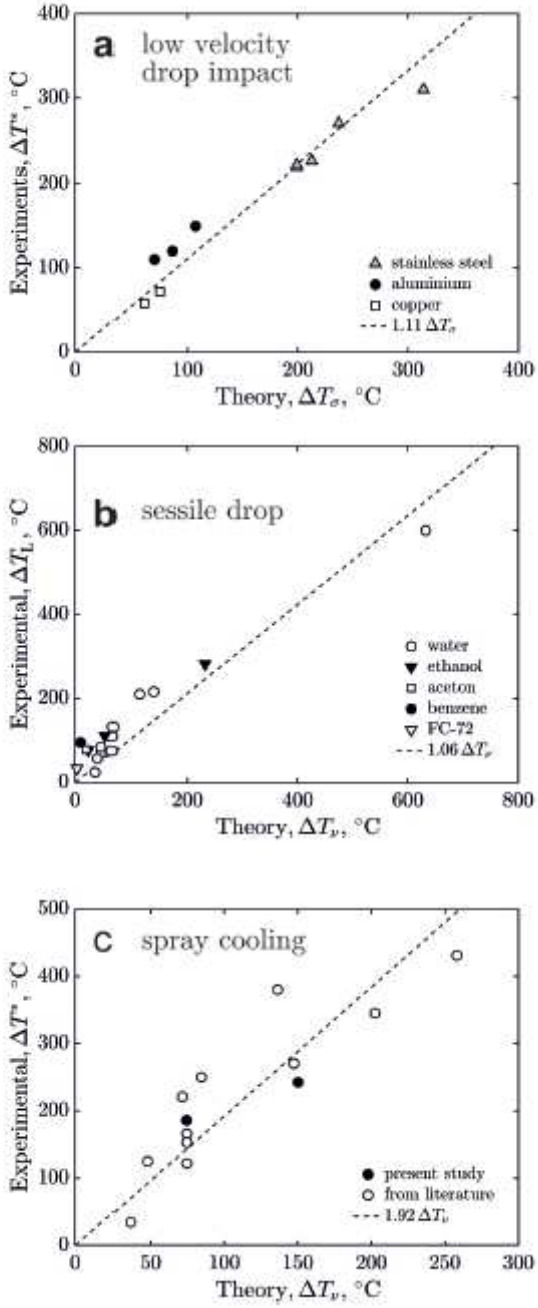

Figure 5

Comparison of the threshold overheat temperatures DT□ □ T□□Tsat with the theoretically predicted scales DTs and DTn . a, Data for low velocity single drop impact withWe < 2:5Re2=5, governed by surface tension, as a function of DTs defined in (8); b, The existing data from the literature for the Leidenfrost point DTL for sessile drops of different liquids and substrates as a function of DTn ; c, Data for water spray cooling of targets of different materials and for the high-speed single drop impacts withWe > 2:5Re2=5, governed by the viscosity, as a function of DTn . The data for different liquids from this study and from the literature are listed in the Supplementary Materials.

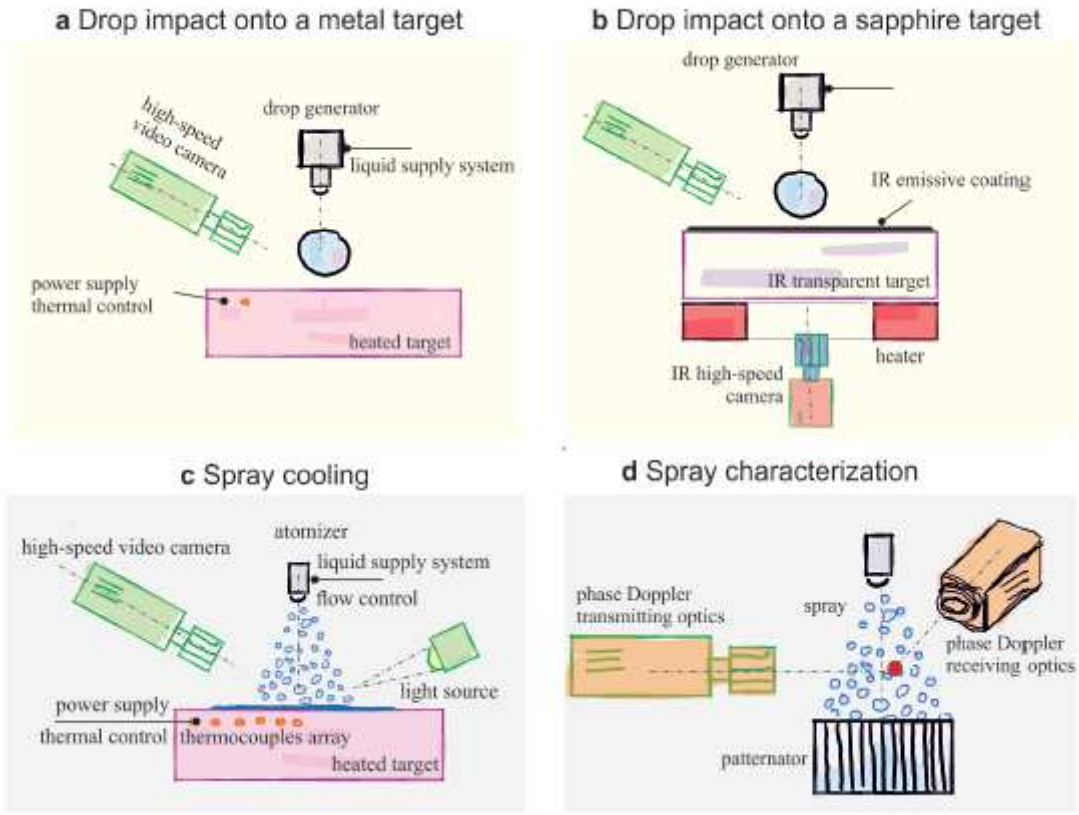

Figure 6

Sketches of the experimental setups for the single drop and spray cooling experiments. a, The setup consists of an adjustable drop generation unit, a heated impact target and a high-speed observation system. The heater and impact target are replaced for IR measurements during the drop impact. b, The setup for infrared (IR) measurements. The heater provides bottom view optical access for a high-speed infrared camera. c, Setup for characterization of spray cooling . d, Setup for detailed spray characterization.

Supplementary Files

This is a list of supplementary files associated with this preprint. Click to download.

- supplemThermalRebound.pdf
- TableS1.png